

# AN ANALYSIS OF SURFACE RELAXATION IN THE SURFACE CAUCHY–BORN MODEL

K. JAYAWARDANA, C. MORDACQ, C. ORTNER, AND H. S. PARK

**ABSTRACT.** The Surface Cauchy–Born (SCB) method is a computational multi-scale method for the simulation of surface-dominated crystalline materials. We present an error analysis of the SCB method, focused on the role of surface relaxation.

In a linearized 1D model we show that the error committed by the SCB method is  $\mathcal{O}(1)$  in the mesh size; however, we are able to identify an alternative “approximation parameter” — the stiffness of the interaction potential — with respect to which the error in the mean strain is exponentially small. Our analysis naturally suggests an improvement of the SCB model by enforcing atomistic mesh spacing in the normal direction at the free boundary.

## 1. INTRODUCTION

Miniaturization of materials to the nanometer scale has led to unexpected and often enhanced mechanical properties that are not found in corresponding bulk materials [4, 28]. The size-dependence of the mechanical behavior and properties has been experimentally observed to begin around a scale of about 100 nanometers [18]. A fully atomistic simulation of a nanostructure of this size would require on the order of  $10^8$  atoms, which motivates the need for computationally efficient multiscale methods.

The underlying cause for the size-dependent mechanical properties is that surface atoms have fewer bonding neighbours, or a coordination number reduction, as compared to atoms that lie within the material bulk. This results in the elastic properties of surfaces being different from those of an idealized bulk material [18], which becomes important with decreasing structural size and increasing surface area to volume ratio [4]. Additionally, nanoscale surface stresses [3], which also arise from the coordination number reduction of surface atoms [30], cause deformation of not only the surfaces, but also the underlying bulk [14], and can result in unique physical properties such as phase transformations [5], or shape memory and pseudoelasticity effects in FCC nanowires that are not observed in the corresponding bulk material [20, 15].

To study surface-dominated nanostructures, Park *et al.* recently developed the surface Cauchy–Born (SCB) model [24, 21, 22]. The idea is to seek an energy functional

---

*Date:* July 26, 2021.

*2000 Mathematics Subject Classification.* 70C20, 70-08, 65N12, 65N30.

*Key words and phrases.* surface-dominated materials, surface Cauchy–Born rule, coarse-graining.

KJ and CM were supported by undergraduate vacation bursaries at the Oxford Centre for Nonlinear PDE. CO was supported by the EPSRC Grant EP/H003096 “Analysis of Atomistic-to-Continuum Coupling Methods”. HP was supported by NSF grants CMMI-0750395 and CMMI-1036460.

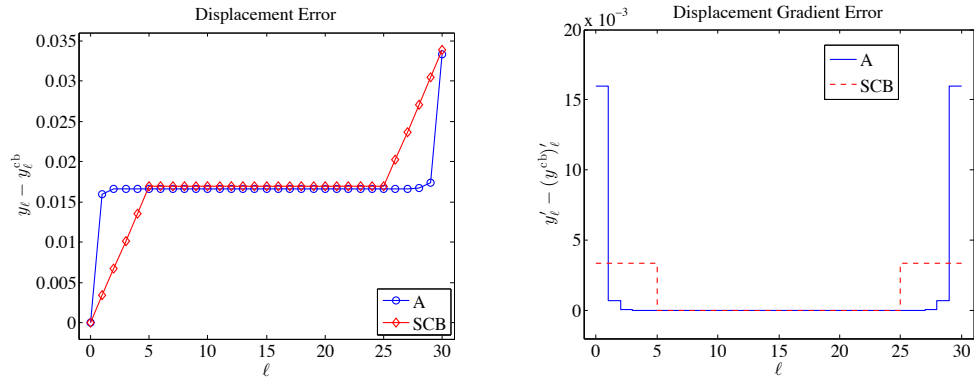


FIGURE 1. Displacements and displacement gradients of an atomistic solution and a surface Cauchy–Born solution, relative to the bulk Cauchy–Born solution, for a 1D model problem. We observe unexpectedly high accuracy at the finite element nodes despite a large error in the displacement gradient.

of the form

$$E^{\text{scb}}(y) = \int_{\Omega} W(\partial y) \, dx + \int_{\partial\Omega} \gamma(\partial y, \nu) \, ds,$$

where  $\Omega \subset \mathbb{R}^3$  is an elastic body,  $y : \Omega \rightarrow \mathbb{R}^3$  a deformation field,  $W$  the bulk stored energy function, and  $\gamma$  a surface stored energy function. The potentials  $W, \gamma$  are chosen such that  $W(\mathbf{F})$  denotes the energy per unit volume in an infinite crystal under the deformation  $y(x) = \mathbf{F}x$ , while  $\gamma(\mathbf{F}, \nu)$  is the surface energy per unit area of a half-space with surface normal  $\nu$ , under the deformation  $y(x) = \mathbf{F}x$ . Thus,  $W$  and  $\gamma$  are *derived* from the underlying atomistic model. For  $W$  this is a well-understood idea [1, 8]; the novel approach in the SCB method is to apply the same principle to the surface energy potential.

In contrast to the SCB method, most computational models (see, e.g., [35, 10, 12]) are based upon a finite element discretization of the governing surface elasticity equations of Gurtin and Murdoch [11], where the constitutive relation for the surface is linearly elastic or uses standard hyperelastic strain energy functions [13].

The SCB model was successfully applied to various nanomechanical boundary value problems, including thermomechanical coupling [33], resonant frequencies, and elucidating the importance of nonlinear, finite deformation kinematics on the resonant frequencies of both FCC metal [23] and silicon nanowires [16, 17], bending of FCC metal [34] nanowires, and electromechanical coupling in surface-dominated nanostructures [19].

The purpose of the present work is to initiate a mathematical analysis of the accuracy of the SCB method. We focus on the simplest setting where the only effect is a surface relaxation in normal direction. While the SCB model does include surface physics that are neglected in the standard Cauchy–Born (CB) model, due to employing a coarse finite element discretisation it does not resolve the resulting boundary layer; see the numerical results in [9] as well as see Figure 1 for a 1D toy model demonstrating this. It is therefore *a priori* unclear to what extent the SCB improves upon the CB model.

Figure 1 suggests that, while the error in the displacement and displacement gradient is indeed of order  $\mathcal{O}(1)$  in the boundary layer, the displacement error in finite element nodes is visually negligible, which would imply that the SCB model approximates the *mean strain* (and possibly other averaged quantities) to a much higher degree of accuracy. This was indeed observed in extensive numerical tests presented in [21, 22, 9].

There is no traditional discretisation or approximation parameter available with respect to which we might try to explain this effect. Instead, our analysis measures the SCB error in terms of the stiffness of the interaction potential. This enables us to identify a suitable asymptotic limit for our analysis on a linearized model problem. We confirm the analytical predictions with numerical experiments on the fully nonlinear problem in 1D and on a periodic semi-infinite 2D domain.

To the best of our knowledge, our work presents the first approximation error results for the SCB method. Although our analysis is elementary, it makes two important novel contributions: 1. We show that the “correct” approximation parameter is the stiffness of the interaction potential (however, Theil [32] uses similar ideas for an analysis of surface relaxation); and 2. We show that the mean strain (which is an important quantity of interest) has a much lower error than the strain field. 3. Our results show how to substantially improve the accuracy of the SCB method at little additional computational cost. Finally, we hope that this work will stimulate further research on computationally efficient multiscale methods for surface-dominated nanostructures.

The issues we address here are closely related to the classical problem of numerical methods for resolving boundary layers [25]. The main difference in our case is the discrete setting which does not give us the opportunity to let the mesh-size tend to zero. For a mathematical analysis of thin atomistic structures, surface energies and surface relaxation we refer to [27, 2, 32, 26] and references therein. Our work also draws inspiration from [6, 7] where a similar linearised model problem is used to analyze the accuracy of atomistic-to-continuum coupling methods.

## 2. ANALYSIS OF A 1D MODEL PROBLEM

**2.1. Atomistic model.** We consider a semi-infinite chain of atoms with reference positions  $\ell \in \mathbb{N}$ , and deformed positions  $y_\ell$ ,  $\ell \in \mathbb{N}$ . We assume that the chain interacts through second-neighbour Morse pair interaction. Hence, a deformed configuration  $y$  has energy

$$E^a(y) := \sum_{\ell=0}^{\infty} \left[ \phi(y_{\ell+1} - y_\ell) + \phi(y_{\ell+2} - y_\ell) \right], \quad (1)$$

where  $\phi$  is a shifted Morse potential with stiffness parameter  $\alpha > 0$  and potential minimum  $r_0 > 0$ ,

$$\phi(r) = \exp(-2\alpha(r - r_0)) - 2\exp(-\alpha(r - r_0)) - \phi_0,$$

where  $\phi_0$  is chosen so that  $W(1) = 0$ , where  $W(r) := \phi(r) + \phi(2r) = 0$ ,  $r_0$  is defined such that  $W'(1) = 0$ ,

$$r_0 = 1 + \frac{1}{\alpha} \log \left( \frac{1 + 2e^{-\alpha}}{1 + 2e^{-2\alpha}} \right), \quad (2)$$

and  $\alpha \geq 1 + \sqrt{3}$  remains a free parameter. This restriction on  $\alpha$  ensures that  $\phi''(2) \leq 0$ , which will be convenient in the analysis. The shift of the potential by  $\phi_0$  ensures that  $E^a$  is well-defined.

The potential  $W$  is called the *Cauchy–Born stored energy density*. We have chosen the parameters in the Morse potential so that 1 is the minimizer of  $W$ , that is, we are working in non-dimensional atomic units.

Since  $E^a$  is translation invariant, it is convenient to fix  $y_0 = 0$ . In that case,  $y_\ell$  is completely determined by the *forward differences*  $y'_\ell := y_{\ell+1} - y_\ell$ . Hence we change coordinates from the deformation  $y_\ell$  to the displacement gradient  $u_\ell := y'_\ell - 1$ , and rewrite  $E^a$  as

$$E^a(u) := \sum_{\ell=0}^{\infty} \left[ \phi(1 + u_\ell) + \phi(2 + u_\ell + u_{\ell+1}) \right].$$

The proof of the next result, which establishes that  $E^a$  is well-defined, is given in the appendix.

**Proposition 1.**  *$E^a$  is well-defined and twice Fréchet differentiable in  $\ell^1(\mathbb{N})$  with first and second variations given by*

$$\begin{aligned} \langle \delta E^a(u), v \rangle &= \sum_{\ell=0}^{\infty} \left[ \phi'(1 + u_\ell) v_\ell + \phi'(2 + u_\ell + u_{\ell+1}) (v_\ell + v_{\ell+1}) \right], \\ \langle \delta^2 E^a(u) v, w \rangle &= \sum_{\ell=0}^{\infty} \left[ \phi''(1 + u_\ell) v_\ell w_\ell + \phi''(2 + u_\ell + u_{\ell+1}) (v_\ell + v_{\ell+1}) (w_\ell + w_{\ell+1}) \right]. \end{aligned}$$

**2.2. The Cauchy–Born and surface Cauchy–Born models.** The Cauchy–Born approximation is designed to model elastic bulk behaviour in crystals. The stored energy density is chosen so that the Cauchy–Born energy is exact under homogeneous deformations in the absence of defects (such as surfaces). For the 1D model (1) this yields

$$E^{\text{cb}}(y) := \int_0^\infty W(y') \, dx, \quad \text{for } y \in W_0^{1,1}(0, \infty), \quad (3)$$

or equivalently, written in terms of the displacement gradient  $u = y' - 1$ ,

$$E^{\text{cb}}(y) = \int_0^\infty W(1 + u) \, dx, \quad \text{for } u \in L^1(0, \infty),$$

where  $W(r) = \phi(r) + \phi(2r)$  was already defined above.

We consider a  $P_1$  finite element discretisation of the Cauchy–Born model. Let  $X_h := \{X_0, X_1, \dots\} \subset \mathbb{N}$  be a strictly increasing sequence of grid points with  $X_0 = 0$ , and let  $h_j := X_{j+1} - X_j$ . A  $P_1$  discretisation of  $y$  corresponds to a  $P_0$  discretisation of the displacement gradient  $u$ , hence we define for  $(U_j)_{j=0}^\infty \subset \mathbb{R}$ , where  $U_j$  denotes the



FIGURE 2. Visualisation of (5): the bond at the bottom of the graph is counted half in the Cauchy–Born model, even though it does not exist in the atomistic model, hence it gives a contribution  $-\frac{1}{2}\phi(2y'(0))$  to the surface energy.

displacement gradient in the element  $(X_j, X_{j+1})$ ,

$$E_h^{\text{cb}}(U) := \sum_{j=0}^{\infty} h_j W(1 + U_j).$$

The Cauchy–Born approximation commits an error at the crystal surface, which the surface Cauchy–Born (SCB) approximation aims to rectify. The idea of the SCB method (in our 1D setting) is to define

$$E_h^{\text{scb}}(y) := \int_0^{\infty} W(y') \, dx + \gamma(y'(0)), \quad (4)$$

and choose  $\gamma$  such that the energy is exact under homogeneous deformations, which yields the formula

$$\gamma(F) := -\frac{1}{2}\phi(2F); \quad (5)$$

see also Figure 2. Converting to the displacement gradient coordinate discretised by the  $P_0$  finite element method we obtain

$$E_h^{\text{scb}}(U) := E_h^{\text{cb}}(U) + \gamma(1 + U_0).$$

**Proposition 2.**  $E_h^{\text{cb}}$  and hence  $E_h^{\text{scb}}$  are well-defined and twice Fréchet differentiable in the weighted space  $\ell_h^1(X_h) := \{V = (V_j)_{j=0}^{\infty}\}$  equipped with the norm

$$\|V\|_{\ell_h^1} := \sum_{j=0}^{\infty} h_j |V_j|.$$

The first and second variations of  $E_h^{\text{scb}}$  are given by

$$\begin{aligned} \langle \delta E_h^{\text{scb}}(U), V \rangle &= \sum_{j=0}^{\infty} h_j W'(1 + U_j) V_j + \gamma'(1 + U_0) V_0, \\ \langle \delta^2 E_h^{\text{scb}}(U) V, W \rangle &= \sum_{j=0}^{\infty} h_j W''(1 + U_j) V_j W_j + \gamma''(1 + U_0) V_0 W_0. \end{aligned}$$

**2.3. Analysis of the linearized models.** The parameter  $r_0$  for the Morse potential was chosen so that 1 is the minimizer of the Cauchy–Born stored energy function, which implies that

$$U_j^{\text{cb}} := 0, \quad \text{for } j = 0, 1, \dots \quad (6)$$

is the ground state of  $E_h^{\text{cb}}$ . More generally,  $u^{\text{cb}} := (0)_{\ell=0}^\infty$  gives the *bulk ground state* of the crystal described by the model (1). We now consider linearisations of  $E_h^{\text{scb}}$  and  $E^{\text{a}}$  about the Cauchy–Born state:  $\delta E(0) + \delta^2 E(0)u = 0$ , where  $E \in \{E^{\text{a}}, E_h^{\text{scb}}\}$ .

From Proposition 2 we obtain the linearised optimality condition for  $E_h^{\text{scb}}$ ,

$$\begin{aligned} \gamma'(1) + (h_0 W''(1) + \gamma''(1))U_0 &= 0, \quad \text{and} \\ h_j W''(1)U_j &= 0 \quad \text{for } j = 1, 2, \dots, \end{aligned}$$

which gives the linearised surface Cauchy–Born solution

$$U_0^{\text{scb}} = \frac{-\gamma'(1)}{h_0 W''(1) + \gamma''(1)}, \quad \text{and} \quad U_j^{\text{scb}} = 0, \quad \text{for } j = 1, 2, \dots \quad (7)$$

From Proposition 1 we obtain the linearised optimality condition for the atomistic model  $E^{\text{a}}$ ,

$$\begin{aligned} \phi'(1) + \phi''(1)u_0 + \phi'(2) + \phi''(2)(u_0 + u_1) &= 0, \\ \phi'(1) + \phi''(1)u_j + 2\phi'(2) + \phi''(2)(u_{j-1} + 2u_j + u_{j+1}) &= 0, \quad j \geq 1, \end{aligned}$$

which, using the fact that  $\phi'(1) + 2\phi'(2) = W'(1) = 0$  can be rewritten in the form

$$\begin{aligned} [\phi''(1) + \phi''(2)]u_0 + \phi''(2)u_1 &= \phi'(2), \\ \phi''(2)u_{\ell-1} + [\phi''(1) + 2\phi''(2)]u_\ell + \phi''(2)u_{\ell+1} &= 0, \quad \ell \geq 1. \end{aligned}$$

This finite difference equation can be easily solved explicitly, which yields the solution

$$u_\ell^{\text{a}} := \frac{\phi'(2)\lambda^\ell}{\phi''(1) + \phi''(2)(1 + \lambda)}, \quad \text{where} \quad \lambda = \frac{\sqrt{1 + 4\frac{\phi''(2)}{\phi''(1)}} - 1 - 2\frac{\phi''(2)}{\phi''(1)}}{2\frac{\phi''(2)}{\phi''(1)}} \quad (8)$$

is the unique solution in  $(0, 1)$  of the characteristic equation

$$\phi''(2)\lambda^2 + [\phi''(1) + 2\phi''(2)]\lambda + \phi''(2) = 0.$$

Since the expressions for (7) and (8) are somewhat bulky we expand them in the stiffness parameter  $\alpha$ . The rationale for expanding in this parameter is that all models should coincide in the limit  $\alpha \rightarrow \infty$ . We hope, however, that our results will also yield useful predictions for moderate  $\alpha$ . The elementary proof is postponed to the appendix.

**Proposition 3.** *Asymptotically as  $\alpha \rightarrow 0$  we have the expansions*

$$U_0^{\text{scb}} = \frac{e^{-\alpha}}{h_0\alpha} \left[ 1 - \left(1 + \frac{2}{h_0}\right)e^{-\alpha} + \mathcal{O}(e^{-2\alpha}) \right], \quad \text{and} \quad (9)$$

$$u_0^{\text{a}} = \frac{e^{-\alpha}}{\alpha} \left[ 1 - 4e^{-\alpha} + \mathcal{O}(e^{-2\alpha}) \right]. \quad (10)$$

**Remark 1.** The asymptotic expansions (9) and (10) justify *a posteriori* the linearisation since they show that the displacements from the Cauchy–Born state are indeed small in the limit as  $\alpha \rightarrow \infty$ .  $\square$

**2.4. Error estimates.** We first note that each  $P_0$  function  $U = (U_j)_{j=0}^\infty$  can be understood as a lattice function  $u = (u_\ell)_{\ell=0}^\infty$  through the interpolation

$$u_\ell = U_j \quad \text{for } \ell = X_j, \dots, X_{j+1} - 1, \quad j \in \mathbb{N}.$$

With this interpolation we obtain  $u^{\text{cb}} = 0$  and  $u^{\text{scb}}$  from the linearized CB and SCB solutions  $U^{\text{cb}}$  and  $U^{\text{scb}}$ , given in (7).

We are interested in the improvement the SCB model gives over the pure Cauchy–Born model, that is, we wish to measure the relative errors

$$\text{Err}_p := \frac{\|u^{\text{scb}} - u^{\text{a}}\|_{\ell^p}}{\|u^{\text{cb}} - u^{\text{a}}\|_{\ell^p}} = \frac{\|u^{\text{scb}} - u^{\text{a}}\|_{\ell^p}}{\|u^{\text{a}}\|_{\ell^p}}.$$

Of particular interest are the uniform error  $\text{Err}_\infty$  and the error in the energy-norm  $\text{Err}_2$ . We shall consider two separate cases:  $h_0 > 1$  and  $h_0 = 1$ .

**Proposition 4 (Strain error).** *Let  $p \in [1, \infty]$  and  $h_0 > 1$ , then*

$$\text{Err}_p = C_p + \mathcal{O}(e^{-\alpha}), \quad (11)$$

where  $\frac{1}{2} \leq C_p \leq 2$ . If  $h_0 = 1$ , then

$$\text{Err}_p = 2^{1/p} e^{-\alpha} + \mathcal{O}(e^{-2\alpha}). \quad (12)$$

*Proof.* We consider the case  $h_0 = 1$  first. In that case (10) gives us

$$\left( \sum_{\ell=1}^{\infty} |u_\ell^{\text{scb}} - u_\ell^{\text{a}}|^p \right)^{1/p} = \left( \sum_{\ell=1}^{\infty} |u_\ell^{\text{a}}|^p \right)^{1/p} = \lambda u_0^{\text{a}} (1 - \lambda^p)^{-1/p},$$

and similarly,  $\|u^{\text{a}}\|_{\ell^p} = u_0^{\text{a}} (1 - \lambda^p)^{-1/p}$ . Using the asymptotic expansions (18) for  $\lambda$  it is straightforward to show that

$$(1 - \lambda^p)^{-1/p} = 1 + \mathcal{O}(\lambda) = 1 + \mathcal{O}(e^{-\alpha});$$

hence employing also (10) we obtain

$$\|u^{\text{a}}\|_{\ell^p} = \frac{e^{-\alpha}}{\alpha} + \mathcal{O}\left(\frac{e^{-2\alpha}}{\alpha}\right), \quad \text{and} \quad \left( \sum_{\ell=1}^{\infty} |u_\ell^{\text{scb}} - u_\ell^{\text{a}}|^p \right)^{1/p} = \frac{e^{-2\alpha}}{\alpha} + \mathcal{O}\left(\frac{e^{-3\alpha}}{\alpha}\right). \quad (13)$$

For  $\ell = 0$ , since  $h_0 = 1$ , we have

$$|u_0^{\text{scb}} - u_0^{\text{a}}| = \left| \frac{e^{-\alpha}}{\alpha} [1 - 3e^{-\alpha} + \mathcal{O}(e^{-2\alpha})] - \frac{e^{-\alpha}}{\alpha} [1 - 4e^{-\alpha} + \mathcal{O}(e^{-2\alpha})] \right| = \frac{e^{-2\alpha}}{\alpha} + \mathcal{O}\left(\frac{e^{-3\alpha}}{\alpha}\right).$$

Combined with (13) this gives

$$\text{Err}_p = \frac{\|u^a - u^{\text{scb}}\|_{\ell^p}}{\|u^a\|_{\ell^p}} = \frac{2^{1/p} \frac{e^{-2\alpha}}{\alpha} + \mathcal{O}\left(\frac{e^{-3\alpha}}{\alpha}\right)}{\frac{e^{-\alpha}}{\alpha} + \mathcal{O}\left(\frac{e^{-2\alpha}}{\alpha}\right)} = 2^{1/p} e^{-\alpha} + \mathcal{O}(e^{-2\alpha}),$$

which concludes the proof of (12).

In the case  $h_0 > 1$  the convenient cancellation of first-order terms in  $u_0^{\text{scb}} - u_0^a$  does not occur. Instead, using (13) we obtain

$$\|u^a - u^{\text{scb}}\|_{\ell^p} = \frac{e^{-\alpha}}{\alpha} \left( \left|1 - \frac{1}{h_0}\right|^p + \sum_{\ell=1}^{X_1-1} \left|\frac{1}{h_0}\right|^p \right)^{1/p} + \mathcal{O}\left(\frac{e^{-2\alpha}}{\alpha}\right)$$

This immediately gives (11).  $\square$

We see from (11) that if we use a coarse finite element mesh up to the boundary, then the error in the displacement gradient will be typically of the order 50% or more. By contrast, if we refine the finite element mesh to atomistic precision at the boundary then the relative error is exponentially small in the stiffness parameter  $\alpha$ .

The quantity  $\text{Err}_p$  measures the error in a pointwise sense. However, in some cases we are only interested in correctly reproducing certain macroscopic quantities such as the mean strain error

$$\overline{\text{Err}} := \left| \frac{\sum_{\ell=0}^{\infty} (u_{\ell}^{\text{scb}} - u_{\ell}^a)}{\sum_{\ell=0}^{\infty} u_{\ell}^a} \right|.$$

Note that, up to higher order terms, this error also bounds the error in the displacements at the finite element nodes, which we observed in Figure 1 to be much smaller than the strain error.

In the following result we confirm that, indeed, the mean strain error is an order of magnitude smaller than the pointwise strain error.

**Proposition 5 (Mean strain error).** *Asymptotically as  $\alpha \rightarrow \infty$ , the mean strain error satisfies*

$$\overline{\text{Err}} = 2\left(1 - \frac{1}{h_0}\right)e^{-\alpha} + \mathcal{O}(e^{-2\alpha}). \quad (14)$$

*Proof.* We first compute the mean strains in the atomistic and the SCB models. For the atomistic model we have

$$\bar{u}^a := \sum_{\ell=0}^{\infty} u_{\ell}^a = \frac{u_0^a}{1 - \lambda}$$

Since  $(1 - \lambda)^{-1} = 1 + e^{-\alpha} + \mathcal{O}(e^{-2\alpha})$  we obtain

$$\bar{u}^a = \frac{e^{-\alpha}}{\alpha} [(1 - 4e^{-\alpha})(1 + e^{-\alpha}) + \mathcal{O}(e^{-2\alpha})] = \frac{e^{-\alpha}}{\alpha} [1 - 3e^{-\alpha} + \mathcal{O}(e^{-2\alpha})],$$

For the SCB model, we have

$$\bar{u}^{\text{scb}} = \sum_{j=0}^{\infty} h_j U_j^{\text{scb}} = h_0 U_0^{\text{scb}} = \frac{e^{-\alpha}}{\alpha} \left[ 1 - \left(1 + \frac{2}{h_0}\right) e^{-\alpha} + \mathcal{O}(e^{-2\alpha}) \right],$$



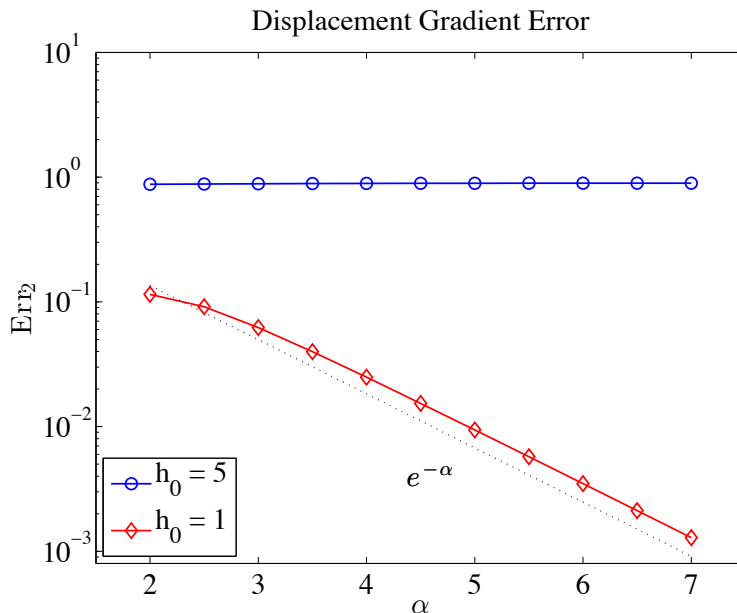


FIGURE 3. Relative error in the  $W^{1,2}$ -seminorm of the 1D nonlinear SCB model for varying stiffness parameter  $\alpha$  and two types of finite element grids; cf. Section 2.5.

and hence the error is given by

$$\bar{u}^{\text{scb}} - \bar{u}^{\text{a}} = 2\left(1 - \frac{1}{h_0}\right) \frac{e^{-2\alpha}}{\alpha} + \mathcal{O}\left(\frac{e^{-3\alpha}}{\alpha}\right).$$

This immediately implies (14).  $\square$

**Remark 2.** Since  $E^{\text{a}}$  and  $E^{\text{scb}}$  are Fréchet differentiable in suitable function spaces it should be possible, using nonlinear analysis techniques such as the inverse function theorem, to extend the results from the linearized model problem to the fully nonlinear problem, provided that the stiffness parameter  $\alpha$  is sufficiently large. Techniques of this kind have been used, for example, in [32].  $\square$

**2.5. Numerical results.** We confirm through numerical experiments that the results of Propositions 4 and 5 are still valid in the nonlinear setting. In these experiments we choose  $r_0 = 1$  instead of (2), choose a finite chain with 31 atoms, and let  $\alpha$  vary between 2 and 7. For experiments with  $h_0 = 5$  the gridpoints for the Cauchy–Born and SCB models are chosen as  $X = (0, 5, 10, \dots, 30)$ . For experiments with  $h_0 = 1$ , the gridpoints are chosen as  $X = (0, 1, 5, \dots, 25, 29, 30)$ .

The results of the experiments are displayed in Figures 3 and 4. All results except for the relative error in the mean strain with  $h_0 = 1$  confirm our analytical results in the linearized case. We have, at present, no explanation why the mean strain error  $\overline{\text{Err}}$  with  $h_0 = 1$  is of the order  $\mathcal{O}(e^{-3\alpha})$  instead of  $\mathcal{O}(e^{-2\alpha})$ . A finer asymptotic analysis in the linearized case would in fact give the expansion  $\overline{\text{Err}} = 2e^{-2\alpha} + \mathcal{O}(e^{-3\alpha})$ .

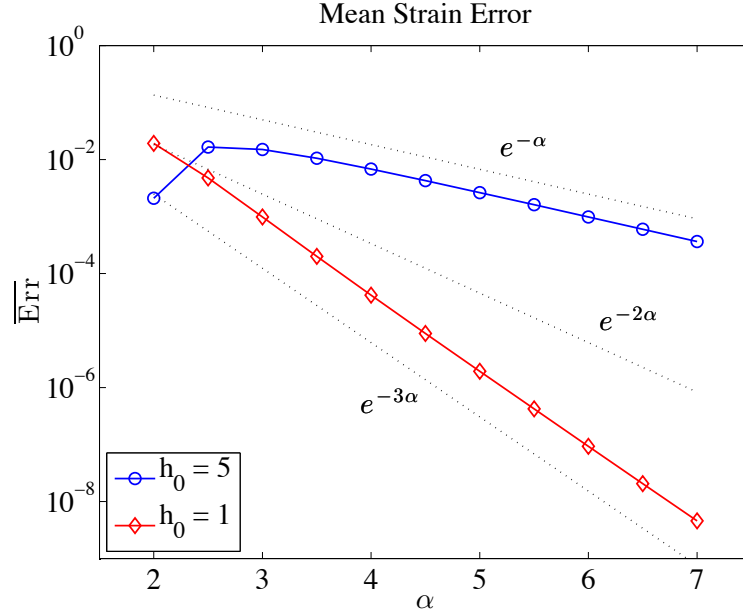


FIGURE 4. Relative error in the mean strain of the 1D nonlinear SCB model for varying stiffness parameter  $\alpha$  and two types of finite element grids; cf. Section 2.5.

### 3. NUMERICAL RESULTS IN 2D

In this section we investigate numerically, to what extent the 1D results might extend to the 2D setting. We will formulate a problem in a semi-infinite strip, where we expect relaxation only in the normal direction to the surfaces. Hence the problem reduces to a 1D problem for the displacements in that direction. The 1D analysis can be applied to this case with only minor changes, and we therefore expect the same behaviour as in the 1D case. This is fully confirmed by the results of our numerical experiment.

**3.1. Formulation of the SCB method.** In 2D one expects (this is rigorously proven only for large stiffness parameter  $\alpha$  [31]) that the ground-state under Morse potential interaction is the triangular lattice. Hence we choose as the atomistic reference configuration a subset  $\Lambda \subset \mathbb{A}\mathbb{Z}^2$ , where

$$\mathbf{A} = \begin{bmatrix} 1 & 1/2 \\ 0 & \sqrt{3}/2 \end{bmatrix}.$$

For future reference, we define  $a_1 := (1, 0)$ ,  $a_2 := (1/2, \sqrt{3}/2)$  and  $a_3 := (-1/2, \sqrt{3}/2)$ , which are the directions of nearest-neighbour bonds.

Specifically, we choose  $N_1, N_2 \in \mathbb{N}$  and define

$$\Lambda := \{\mathbf{A}(n_1, n_2)^T \in \mathbb{Z}^2 \mid 1 < n_1 \leq N_1, 0 \leq n_2 \leq N_2\},$$

as the periodic cell of the semi-infinite strip  $\Lambda^\# := \{\mathbf{A}(n_1, n_2)^T \in \mathbb{Z}^2 \mid 0 \leq n_2 \leq N_2\}$ ; cf. Figure 5. The corresponding continuous domain is  $\Omega := \mathbf{A}((0, N_1] \times (0, N_1])$ .

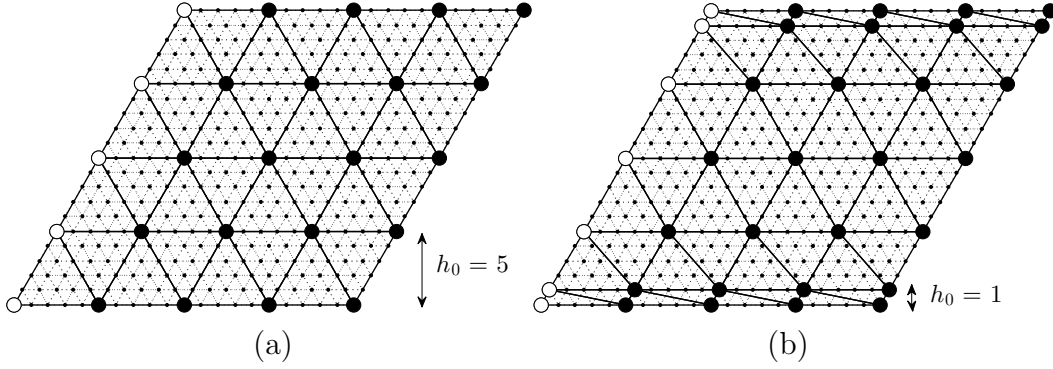


FIGURE 5. Computational domain used in the numerical experiment described in Section 3. The small disks denote the set  $\Lambda$ ; the dotted grid is the micro-triangulation  $\mathcal{T}_a$ ; the large black disks denote the finite element nodes; the large white discs denote finite element nodes that are periodically repeated; the black lines denote the macro-triangulation  $\mathcal{T}_h$ .

An admissible deformed configuration is a map  $y : \Lambda^\# \rightarrow \mathbb{R}^2$ , which is periodic in the  $a_1$ -direction, that is,  $y(\xi + N_1 a_1) = y(\xi) + N_1 a_1$ .

For simplicity we consider only second-neighbour interactions (measured in hopping distance). For each  $\xi \in \Lambda$  let  $\mathcal{N}_\xi := \{\eta \in \Lambda^\# \mid |\eta - \xi| \leq 2\}$  denote the interaction neighbourhood of  $\xi$ , then the potential energy of a deformed configuration is given by

$$E^a(y) := \sum_{\xi \in \Lambda} \frac{1}{2} \sum_{\eta \in \mathcal{N}_\xi} \phi(|y(\eta) - y(\xi)|),$$

where  $\phi$  is again the Morse potential.

To evaluate the deformation gradient  $\partial y$  of a discrete deformation  $y$ , we note that  $\Lambda^\#$  has a natural triangulation  $\mathcal{T}_a$  (see Figure 5), and identify  $y$  with its continuous piecewise affine interpolant in  $P_1(\mathcal{T}_a; \mathbb{R}^2)$ .

Let  $\mathcal{T}_h$  be a *coarse* triangulation of  $\Omega$  (which can be repeated periodically) and let  $P_1(\mathcal{T}_h; \mathbb{R}^2)$  denote the space of continuous and piecewise affine deformations of  $\Omega$ , such that  $y_h(x + N_1 a_1) = y_h(x) + N_1 a_1$ , then the SCB energy of a deformation  $y_h \in P_1(\mathcal{T}_h; \mathbb{R}^2)$  is given by

$$E^{\text{scb}}(y_h) = \int_{\Omega} W(\partial y_h) dx + \int_{\Gamma} \gamma(\partial y_h, \nu) dx,$$

where  $\Gamma \subset \partial\Omega$  denotes the free boundary, that is the portion of the boundary with normal  $\nu = \pm(0, 1)$ ,  $W$  is the Cauchy–Born stored energy function and  $\gamma$  the SCB surface energy function, which are defined as follows:

- If we denote by  $\mathcal{N}_{\text{cb}}$  the interaction neighbourhood of the origin in the infinite lattice  $\mathbf{AZ}^2$  (see Figure 6(a)), then the Cauchy–Born stored energy function is given by

$$W(F) = \frac{1}{\det \mathbf{A}} \sum_{\eta \in \mathcal{N}_{\text{cb}}} \phi(|F\eta|).$$

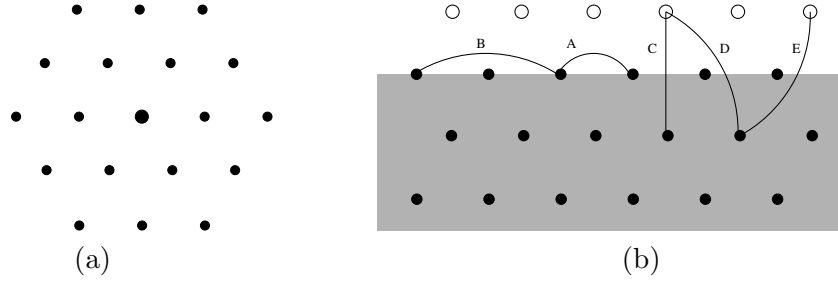


FIGURE 6. (a) Third interaction neighbourhood. (b) Construction of  $\gamma$ : Bonds A, B are underestimated by the Cauchy–Born approximation (counted only half), while the bonds C, D, E are overestimated (they do not exist in the atomistic model but are counted half in the Cauchy–Born model).

- To define  $\gamma$ , we assume throughout that all surfaces of  $\Omega$  are aligned with one of the three directions  $a_1, a_2$ , or  $a_3$ , that is,  $\nu \perp a_j =: \nu^\perp$ . Then the requirement that the SCB energy is exact under homogeneous deformations, in domains without corners, yields the expression

$$\begin{aligned} \gamma(\mathbf{F}, \gamma) &= \frac{1}{2}\phi(|\mathbf{F}\nu^\perp|) + \frac{1}{2}\phi(2|\mathbf{F}\nu^\perp|) \\ &\quad - \frac{1}{2}\phi(\sqrt{3}|\mathbf{F}\nu|) - \frac{1}{2}\phi(2|\mathbf{F}\mathbf{Q}_{12}\nu|) - \frac{1}{2}\phi(2|\mathbf{F}\mathbf{Q}_{12}^T\nu|), \end{aligned}$$

where  $\mathbf{Q}_{12}$  denotes a rotation through arclength  $2\pi/12$ ; see Figure 6(b) for an illustration. A rigorous proof of this formula follows immediately from Shapeev’s bond density lemma [29].

**3.2. Numerical results.** In the numerical experiments we consider two types of finite element grids: a uniform grid with spacing  $h = h_0 = 5$  (cf. Figure 5(a)), and a grid with an additional layer of elements at the free boundary, atomic spacing  $h_0 = 1$  in the normal direction and uniform spacing  $h = 5$  in the tangential direction (cf. Figure 5(b)). We will again measure the following relative errors:

$$\text{Err}_2 := \frac{\|\partial y_h^{\text{scb}} - \partial y^{\text{a}}\|_{L^2}}{\|\partial y_h^{\text{cb}} - \partial y^{\text{a}}\|_{L^2}}, \quad \text{and} \quad \overline{\text{Err}} := \left| \frac{\int_{\Omega} (\partial y_h^{\text{scb}} - \partial y^{\text{a}}) \, dx}{\int_{\Omega} (\partial y_h^{\text{cb}} - \partial y^{\text{a}}) \, dx} \right|,$$

where  $y^{\text{a}}, y_h^{\text{scb}}$ , and  $y_h^{\text{cb}}$  denote the minimizers of, respectively,  $E^{\text{a}}, E^{\text{scb}}$ , and  $E^{\text{cb}}$  with  $\gamma = 0$ . That is,  $\text{Err}_2$  and  $\overline{\text{Err}}$  measure the improvement of SCB over the pure Cauchy–Born model.

The numerical results are displayed in Figures 7 and 8. Although the numerical results do not as clearly display the predicted convergence rates, they do seem to approach these rates for increasing values of  $\alpha$ . What is again clear is that the average strain has a much higher accuracy than the strain field, and that the additional mesh layer also substantially improves the accuracy of the method. We also note that we now observe essentially the predicted rate  $e^{-2\alpha}$  for the mean-strain error of the enhanced SCB model, instead of the unexpected rate  $e^{-3\alpha}$ .

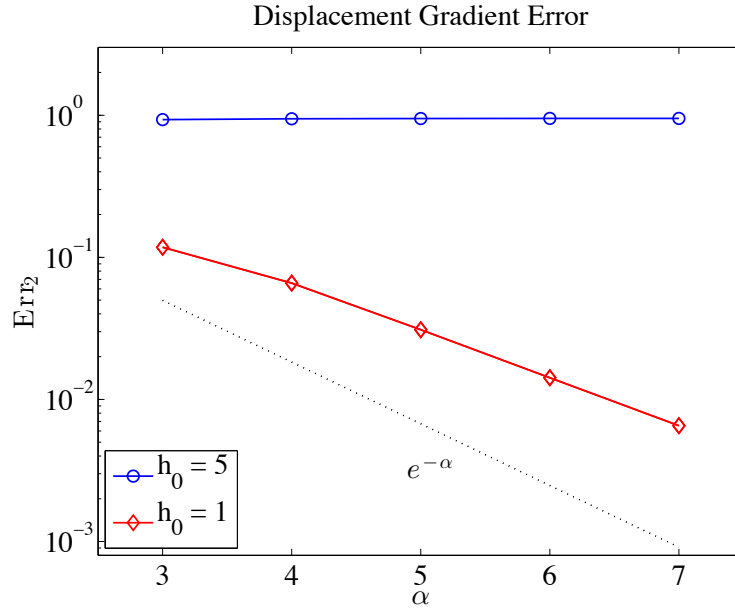


FIGURE 7. Relative error in the  $W^{1,2}$ -seminorm of the 2D SCB model in the flat interface example described in Section 3, for varying stiffness parameter  $\alpha$  and two types of finite element grids.

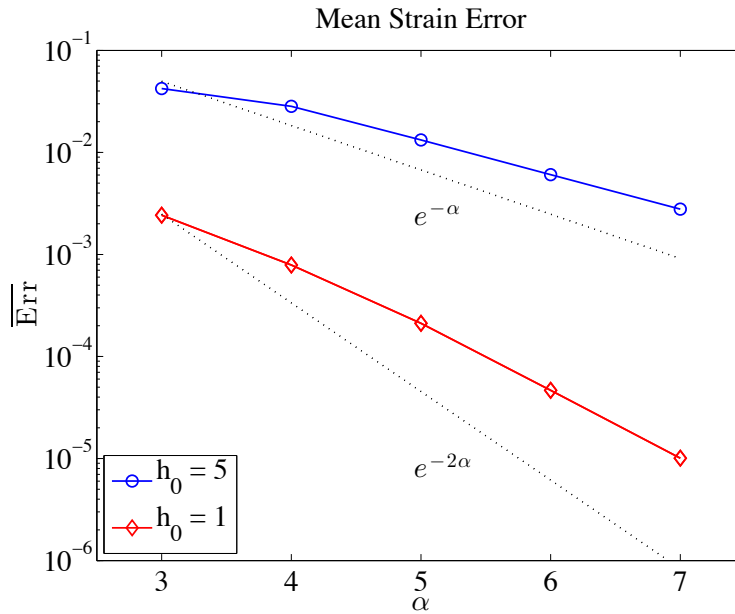


FIGURE 8. Relative error for the mean strain of the 2D SCB model applied to the flat interface example described in Section 3, for varying stiffness parameter  $\alpha$  and two types of finite element grids.

## CONCLUSION

We presented an error analysis of the SCB method in the case where the dominant effect is surface relaxation in the normal direction. Our main results are: 1. We

showed that the “correct” approximation parameter is the stiffness of the interaction potential. 2. We showed that the mean strain (which is an important quantity of interest) has a much lower error than the strain field. 3. We showed that adding a single mesh layer at the free boundary with atomic spacing in the normal direction yields a substantial improvement to the accuracy of the SCB method with minimal increase in the computational cost.

We also performed numerical experiments for domains with corners, which remain inconclusive so far. At corners there is an interplay between the normal stress and tangential stress of adjacent edges, which creates additional elastic fields. A finer analysis of this case is still required. In particular, it would be interesting to understand whether normal or tangential forces dominate the behaviour of the system in that case.

## APPENDIX A. PROOFS

*Proof of Propositions 1 and 2.* For each  $\ell \in \mathbb{N}$  we have

$$\begin{aligned} \phi(1 + u_\ell) + \phi(2 + u_\ell + u_{\ell+1}) &= \phi(1) + \phi'(1)u_\ell + \frac{1}{2}\phi''(\theta_\ell^{(1)})|u_\ell|^2 \\ &\quad + \phi(2) + \phi'(2)(u_\ell + u_{\ell+1}) + \frac{1}{2}\phi''(\theta_\ell^{(2)})|u_\ell + u_{\ell+1}|^2. \end{aligned}$$

where  $(\theta_\ell^{(j)} - j) \in \ell^1$  by Taylor’s theorem. Since  $\phi(1) + \phi(2) = 0$ , summing over  $\ell \in \mathbb{N}$  and noting that the first-order terms cancel, yields

$$E^a(y) \leq C\|u\|_{\ell^2}^2.$$

Note that this seemingly requires only that  $u \in \ell^2$ , however, the series converges absolutely only if  $u \in \ell^1$ .

Repeating the argument for a perturbation from a general state  $E^a(u + v)$  shows the Fréchet differentiability of  $E^a$ .

The same argument can be applied to prove Proposition 2.  $\square$

*Proof of Proposition 3.* Inserting the definition of  $r_0$  from (2) into  $\phi''(1)$  yields

$$\begin{aligned} \phi''(1) &= 4\alpha^2 e^{-2\alpha(1-r_0)} - 2\alpha^2 e^{-\alpha(1-r_0)} \\ &= 4\alpha^2 \left( \frac{1 + 2e^{-\alpha}}{1 + 2e^{-2\alpha}} \right)^2 - 2\alpha^2 \left( \frac{1 + 2e^{-\alpha}}{1 + 2e^{-2\alpha}} \right). \end{aligned}$$

Expanding

$$\frac{1 + 2e^{-\alpha}}{1 + 2e^{-2\alpha}} = 1 + 2e^{-\alpha} + \mathcal{O}(e^{-2\alpha}),$$

we obtain

$$\begin{aligned} \phi''(1) &= 4\alpha^2(1 + 4e^{-\alpha}) - 2\alpha^2(1 + 2e^{-\alpha}) + \mathcal{O}(\alpha^2 e^{-2\alpha}) \\ &= 2\alpha^2 + 12\alpha^2 e^{-\alpha} + \mathcal{O}(\alpha^2 e^{-2\alpha}). \end{aligned} \tag{15}$$

Similar calculations yield the expansions

$$\phi'(2) = 2\alpha e^{-\alpha} + 2\alpha e^{-2\alpha} + \mathcal{O}(\alpha e^{-3\alpha}), \quad \text{and} \tag{16}$$

$$\phi''(2) = -2\alpha^2 e^{-\alpha} + \mathcal{O}(\alpha^2 e^{-3\alpha}). \tag{17}$$

Writing out  $U_0^{\text{scb}}$  in terms of the Morse potential, and using the fact that  $2 \leq 4 - 2/h_0 \leq 4$ , which ensures that  $\phi''(1) + (4 - 2/h_0)\phi''(2) \geq W''(1) > 0$ , we obtain

$$\begin{aligned} h_0 U_0^{\text{scb}} &= \frac{\phi'(2)}{\phi''(1) + (4 - 2/h_0)\phi''(2)} = \frac{\phi'(2)}{\phi''(1)} \frac{1}{1 + (4 - 2/h_0)\frac{\phi''(2)}{\phi''(1)}} \\ &= \frac{\phi'(2)}{\phi''(1)} \left[ 1 - \left(4 - \frac{2}{h_0}\right) \frac{\phi''(2)}{\phi''(1)} + \mathcal{O}\left(\left(\frac{\phi''(2)}{\phi''(1)}\right)^2\right) \right]. \end{aligned}$$

Inserting the expansions (15) to (17) gives (9).

To prove (10) we first expand  $\lambda$  in terms of  $\beta := \frac{\phi''(2)}{\phi''(1)}$ , and then in terms of  $e^{-\alpha}$ ,

$$\begin{aligned} \lambda &= \frac{1}{2\beta} \left( \sqrt{1 + 4\beta} - 1 - 2\beta \right) \\ &= \frac{1}{2\beta} \left( 1 + \frac{1}{2}(4\beta) - \frac{1}{8}(4\beta)^2 + \frac{1}{16}(4\beta)^3 + \mathcal{O}(\beta^4) - 1 - 2\beta \right) \\ &= -\beta + 2\beta^2 + \mathcal{O}(\beta^3) = e^{-\alpha} - 4e^{-2\alpha} + \mathcal{O}(e^{-3\alpha}). \end{aligned} \tag{18}$$

Inserting this result into (8) and a brief computation yield

$$u_0^{\text{a}} = \frac{\phi_2'}{\phi_1'' + \phi_2''(1 + \lambda)} = \frac{e^{-\alpha}}{\alpha} - 4\frac{e^{-2\alpha}}{\alpha} + \mathcal{O}\left(\frac{e^{-3\alpha}}{\alpha}\right).$$

Since  $u_\ell^{\text{a}} = u_0^{\text{a}}\lambda^{-\ell}$  the result (10) follows easily.  $\square$

## REFERENCES

- [1] X. Blanc, C. Le Bris, and P.-L. Lions. From molecular models to continuum mechanics. *Arch. Ration. Mech. Anal.*, 164(4):341–381, 2002.
- [2] A. Braides and M. Cicalese. Surface energies in nonconvex discrete systems. *Math. Models Methods Appl. Sci.*, 17(7):985–1037, 2007.
- [3] R C Cammarata. Surface and interface stress effects in thin films. *Progress in Surface Science*, 46(1):1–38, 1994.
- [4] S Cuenot, C Frétiigny, S Demoustier-Champagne, and B Nysten. Surface tension effect on the mechanical properties of nanomaterials measured by atomic force microscopy. *Physical Review B*, 69:165410, 2004.
- [5] J Diao, K Gall, and M L Dunn. Surface-stress-induced phase transformation in metal nanowires. *Nature Materials*, 2(10):656–660, 2003.
- [6] M. Dobson and M. Luskin. An analysis of the effect of ghost force oscillation on quasicontinuum error. *M2AN Math. Model. Numer. Anal.*, 43(3):591–604, 2009.
- [7] M. Dobson, M. Luskin, and C. Ortner. Accuracy of quasicontinuum approximations near instabilities. *J. Mech. Phys. Solids*, 58(10):1741–1757, 2010.
- [8] W. E and P. Ming. Cauchy-Born rule and the stability of crystalline solids: static problems. *Arch. Ration. Mech. Anal.*, 183(2):241–297, 2007.
- [9] M Farsad, F J Vernerey, and H S Park. An extended finite element/level set method to study surface effects on the mechanical behavior and properties of nanomaterials. *International Journal for Numerical Methods in Engineering*, 84:1466–1489, 2010.
- [10] W Gao, SW Yu, and GY Huang. Finite element characterization of the size-dependent mechanical behaviour in nanosystems. *Nanotechnology*, 17(4):1118–1122, 2006.
- [11] M E Gurtin and A Murdoch. A continuum theory of elastic material surfaces. *Archives of Rational Mechanics and Analysis*, 57:291–323, 1975.

- [12] J He and C M Lilley. The finite element absolute nodal coordinate formulation incorporated with surface stress effect to model elastic bending nanowires in large deformation. *Computational Mechanics*, 44:395–403, 2009.
- [13] A Javili and P Steinmann. A finite element framework for continua with boundary energies. part I: the two-dimensional case. *Computer Methods in Applied Mechanics and Engineering*, 198:2198–2208, 2009.
- [14] H Liang, M Upmanyu, and H Huang. Size-dependent elasticity of nanowires: nonlinear effects. *Physical Review B*, 71:241403(R), 2005.
- [15] W Liang, M Zhou, and F Ke. Shape memory effect in Cu nanowires. *Nano Letters*, 5(10):2039–2043, 2005.
- [16] H S Park. Surface stress effects on the resonant properties of silicon nanowires. *Journal of Applied Physics*, 103:123504, 2008.
- [17] H S Park. Quantifying the size-dependent effect of the residual surface stress on the resonant frequencies of silicon nanowires if finite deformation kinematics are considered. *Nanotechnology*, 20:115701, 2009.
- [18] H S Park, W Cai, H D Espinosa, and H Huang. Mechanics of crystalline nanowires. *MRS Bulletin*, 34(3):178–183, 2009.
- [19] H S Park, M Devel, and Z Wang. A new multiscale formulation for the electromechanical behavior of nanomaterials. *Computer Methods in Applied Mechanics and Engineering*, 200:2447–2457, 2011.
- [20] H S Park, K Gall, and J A Zimmerman. Shape memory and pseudoelasticity in metal nanowires. *Physical Review Letters*, 95:255504, 2005.
- [21] H S Park and P A Klein. Surface cauchy-born analysis of surface stress effects on metallic nanowires. *Physical Review B*, 75:085408, 2007.
- [22] H S Park and P A Klein. A surface cauchy-born model for silicon nanostructures. *Computer Methods in Applied Mechanics and Engineering*, 197:3249–3260, 2008.
- [23] H S Park and P A Klein. Surface stress effects on the resonant properties of metal nanowires: The importance of finite deformation kinematics and the impact of the residual surface stress. *Journal of the Mechanics and Physics of Solids*, 56:3144–3166, 2008.
- [24] H S Park, P A Klein, and G J Wagner. A surface cauchy-born model for nanoscale materials. *International Journal for Numerical Methods in Engineering*, 68:1072–1095, 2006.
- [25] H.-G. Roos, M. Stynes, and L. Tobiska. *Robust numerical methods for singularly perturbed differential equations*, volume 24 of *Springer Series in Computational Mathematics*. Springer-Verlag, Berlin, second edition, 2008. Convection-diffusion-reaction and flow problems.
- [26] L. Scardia, A. Schlömerkemper, and C. Zanini. Boundary layer energies for nonconvex discrete systems. *Math. Models Methods Appl. Sci.*, 21(4):777–817, 2011.
- [27] B. Schmidt. On the passage from atomic to continuum theory for thin films. *Arch. Ration. Mech. Anal.*, 190(1):1–55, 2008.
- [28] J-H Seo, Y Yoo, N-Y Park, S-W Yoon, H Lee, S Han, S-W Lee, T-Y Seong, S-C Lee, K-B Lee, P-R Cha, H S Park, B Kim, and J-P Ahn. Superplastic deformation of defect-free au nanowires by coherent twin propagation. *Nano Letters*, 11:3499–3502, 2011.
- [29] A. V. Shapeev. Consistent energy-based atomistic/continuum coupling for two-body potentials in one and two dimensions. *Multiscale Model. Simul.*, 9(3):905–932, 2011.
- [30] C Q Sun, B K Tay, X T Zeng, S Li, T P Chen, J Zhou, H L Bai, and E Y Jiang. Bond-order-bond-length-bond-strength (bond-OLS) correlation mechanism for the shape-and-size dependence of a nanosolid. *Journal of Physics: Condensed Matter*, 14:7781–7795, 2002.
- [31] F. Theil. A proof of crystallization in two dimensions. *Comm. Math. Phys.*, 262(1):209–236, 2006.
- [32] F. Theil. Surface energies in a two-dimensional mass-spring model for crystals. *ESAIM Math. Model. Numer. Anal.*, 45(5):873–899, 2011.
- [33] G Yun and H S Park. A multiscale, finite deformation formulation for surface stress effects on the coupled thermomechanical behavior of nanomaterials. *Computer Methods in Applied Mechanics and Engineering*, 197:3337–3350, 2008.



- [34] G Yun and H S Park. Surface stress effects on the bending properties of fcc metal nanowires. *Physical Review B*, 79:195421, 2009.
- [35] J Yvonnet, H Le Quang, and Q-C He. An XFEM/level set approach to modelling surface/interface effects and to computing the size-dependent effective properties of nanocomposites. *Computational Mechanics*, 42:119–131, 2008.

K. JAYAWARDANA, DEPARTMENT OF MATHEMATICS, UNIVERSITY COLLEGE LONDON, GOWER STREET, LONDON WC1E 6BT, UK  
*E-mail address:* k.guruge@ucl.ac.uk

C. MORDACQ  
*E-mail address:* Christelle.Mordacq@gmail.com

C. ORTNER, MATHEMATICS INSTITUTE, ZEEMAN BUILDING, UNIVERSITY OF WARWICK, COVENTRY CV4 7AL, UK  
*E-mail address:* christoph.ortner@warwick.ac.uk

H. S. PARK, BOSTON UNIVERSITY, DEPARTMENT OF MECHANICAL ENGINEERING, 730 COMMONWEALTH AVENUE, ENA 212, BOSTON, MA 02215, USA  
*E-mail address:* parkhs@acs.bu.edu